Int. J. Electrochem. Sci., 7 **(2012)** 8832 - 8847

International Journal of ELECTROCHEMICAL SCIENCE
www.electrochemsci.org

Ultrasonic Synthesis: Structural, Optical and Electrical Correlation of TiO_2 Nanoparticles

I. Hernández-Perez[1,2], A. M. Maubert[1], Luis Rendón[3], Patricia Santiago[3], H. Herrera-Hernández[1], L. Díaz-Barriga Arceo[4], V. Garibay Febles[5], Eduardo Palacios González[5], L. González-Reyes[1]*

[1] Universidad Autónoma Metropolitana-Azcapotzalco, Departamento de Ciencias Básicas, Av. San Pablo No. 180, Col. Reynosa Tamaulipas, México, D.F. 02200, México
[2] Universidad Autónoma Metropolitana-Lerma, Departamento de Ciencias Básicas, Av. Hidalgo Pte. No. 46, Lerma, Estado de México 52000, México.
[3] Instituto de Física, UNAM, Circuito de la Investigación Científica s/n, Ciudad Universitaria, Coyoacán 04510, México, D.F., México
[4] Instituto Politécnico Nacional, Departamento de Ingeniería Metalúrgica y Materiales, ESIQIE-UPALM, México, D.F. 07738, México
[5] Instituto Mexicano del Petróleo, Laboratorio de Microscopia de Ultra Alta Resolución, Eje Central Lázaro Cárdenas Norte 152 Col. San Bartolo Atepehuacán, México, D.F. 07730, México
[*]E-mail: leogonzalez@ipn.mx

Received: 18 May 2012 / *Accepted:* 26 July 2012 / *Published:* 1 September 2012

Sonochemical synthesis of nanometric anatase phase has been successfully produced at room temperature by using a simple and environment-friendly method. The effect of the heat treatment on the structural properties of the as-prepared sample has been evaluated and discussed in this research by X-ray powder diffraction and transmission electron microscopy techniques. The structural properties are expected to be strongly correlated with the optical band gap and electrical properties. The results show that the average size of nanocrystallites is in the order of 5 nm with large surface area, where as the system presents pores at the junctions of crystallites. Optical band gap of as-prepared sample has a blue shift, which could be attributed to a quantum size effect. The heat-treated reveals structural changes from anatase to rutile structure at 550 °C. Crystal size increase from 5 to 35 nm, in which anatase and rutile phases coexist. However, by electrochemical technique the high current-charge magnitude is observed in samples with crystallite size of 17 nm but if anatase and rutile are simultaneously present the conductivity decreased. This phenomenon is observed if the difference between anatase and rutile is about 36% in size, indicating that the conduction and valence bands could be further away in the sample.

Keywords: TiO_2; Thermal effects; Sonochemistry, Raman; Electrochemical technique, Electron microscopy

1. INTRODUCTION

Titanium dioxide (TiO_2) in both modifications, anatase (tetragonal *I4/amd*) or rutile phase (tetragonal $P4_2/mnm$), is one of the most important materials for applications based on photon excitation in environmental purification [1,2]. Each phase exhibits different physical properties, which are determined by their structural, chemical and optoelectronic properties; which mean that properties of nanoparticles are often size-dependent [3]. When the size of a semiconductor particle is decreased to the extent that the relative proportions of the surface and bulk regions of the particle are comparable, its energy band structure becomes discrete and will exhibit chemical and optical properties different from those of the bulk material [4]. Thus, the challenge for materials scientific is to find a processing method in which the crystalline phase as well as the size and morphology of TiO_2 nanocrystals can be controlled. The relative simple sol-gel method is the most widely used but unfortunately the sol-gel-method derived precipitates are usually amorphous in nature, which requires further heat treatment to induce crystallization. The heat treatment frequently gives rise to particle agglomeration and grain growth. While the hydrothermal technique is widely employed to enhance crystallinity but a longer aging time is required to obtain crystalline TiO_2 at low temperatures.

Sonochemical synthesis has proven to be a useful technique for generating novel materials with unusual properties and environment-friendly. The sonochemical effects of ultrasound arise from acoustic cavitation, i.e., the formation, growth, and implosive collapse of bubble generates localized hot spots through adiabatic compression or shock wave formation within the gas phase of the collapsing bubble. In this way, sonochemical synthesis allows the major control of crystalline structure, size and morphology of particles [5-9]. Thus, with (sonochemical synthesis) it was possible to prepare large amounts (>90% yield) of pure anatase phase nanoparticles with the choice of a suitable precursor and appropriated experimental conditions. Additionally, with ultrasonic radiation assisted synthesis the time span involved is only 30-60 min. [10]. This method allows the preparation of large amounts of anatase phase in a very short time period and also successive reactions can be performed simultaneously. Sonochemistry is a promising preparation method that may resolve the problems arising from the conventional synthesis methods. Furthermore, this method can save energy and time and, thus reduce the cost of final products. The synthesis is rapid and reproducible compared to the conventional methods, mentioned previously.

The aim of the present investigation is to systematically study the conditions suitable for large scale synthesis of polymorphic materials nanostructures at low temperatures by the choice of a suitable precursor using sonochemistry. From the synthesis nanoparticles of anatase TiO_2 (as-prepared sample) was obtained. Then, this sample was subject to thermal treatment to obtain products with variable anatase-rutile ratio. Extensive spectroscopies were used and electron microscopy (SEM, TEM, and HRTEM) has been carried out in great detail to understand the nature and relationship of the nanostructures synthesized as well as to characterize them in detail. For this purpose the as-prepared sample was heat-treated in order to follow the structural changes due to thermal effects and correlated the results with its optical bandgap, and electrical properties during the phase transformation anatase-to-rutile. The results are present and discussed herein.

2. EXPERIMENTAL DETAILS

2.1. Materials and Methods

The organic compound reactive $[(CH_3)_2CHO]_4Ti$ (TTIP, Aldrich) was used as titanium source. TTIP (150 mL) was mixed with acetone (30 mL) and methanol (30 mL) and subjected to sonochemical treatment for 40 minutes in an ultrasonic clean bath at 38 kHz. Acetone-methanol mixture was used as pressure-transmitting media. The solvents were evaporated from the mix using a magnetic mixer-heater set at 60 ºC until the remaining material has a liquid free, thus dry, appearance. The dried product reference will be along this paper as-prepared sample.

2.2. Heat Treatment

The as-prepared sample was thermally treated in a temperature ranging from 400 to 900 ºC for 2 hours at each temperature. The thermal treatment was carried out in a conventional electrical resistance furnace an under ambient atmosphere at a rate of 10 ºC min^{-1}. After heat treatment ten samples were obtained and they are identified for its temperature range along this paper.

2.3. Characterization Methods

The X-ray diffraction (XRD) patterns were obtained with a Bruker D8 Focus powder diffractometer operating in the reflection mode with Cu-Kα radiation (35 kV, 25 mA) at 2º s^{-1} scan rate. The diffraction patterns for both anatase and rutile powders were compared with reference to database cards ICDD PDF 21-1272 (anatase) and ICDD PDF 21-1276 (rutile). The Scherrer´s equation was used to estimate the crystallite size. The anatase (W_A) phase content or that of rutile (W_R), was calculated from the integrated intensities of anatase (101) ($2\theta = 25.28º$) and rutile (110) ($2\theta = 27.45º$) peaks by the method reported by Spurr-Myers [11]. The Raman Spectroscopy (RS) was conducted on a thermo Nicolet apparatus model Almega, laser-equipped with a 532 nm wavelength using medium intensity and a 1 cm^{-1} shift and a 0.5 cm^{-1} resolution. UV-vis absorption spectra in the profile reflectance mode, dual-beam Varian Cary I spectrophotometer, were used to determine the optical band gap by a graphical method according to the following criterion: plotting $(\alpha h\nu)^n$ versus $h\nu$, and extrapolating the linear region of the plot toward low energies. Here, n=2 for allowed direct transition, n=1/2 for allowed indirect transition. Coarsening and grain growth evolution were analyzed by Transmission Electron Microscopy (TEM) with a JEOL-2000FXI operated at 200 kV and for High Resolution Transmission Electron Microscope (HRTEM) and for a detail analysis about crystal structure was used a Tecnai G2 F30 operated at 300 kV for High Resolution Transmission Electron Microscope. Scanning Electron Microscopy (SEM) was conducted with a Phillips XL-30 operated at 20 kV to determine the morphological changes of anatase as a function of the heat treatment temperature. The Braunauer-Emmett-Teller specific surface area (S_{BET}) of the samples was determined through nitrogen adsorption (Micromeritics ASAP 2000). All the samples were degassed at 100°C for 24 h before measurements.

2.4. Electrical and charge measurements (i-E)

The TiO_2-carbon paste electrodes (TCPE) were prepared with graphite powder (Alfa Aesar) as a conducting agent, silicon oil and TiO_2 at 20%wt as an active material. Then, the mixture of TiO_2 (as-prepared and obtained by thermal treatment samples) was mechanically homogenized and inserted in a 2mm-diameter cylinder (0.0314cm^2). The electrical contact on the TCPE was made with a platinum wire. *i-E* measurements were performed in a conventional three electrodes cell employing cyclic voltammetry (CV) technique a scan rate of 50 mVs-1 using a Potentiostat, Autolab PGSTAT302. The *i-E* performances were carried out in a 0.5M H_2SO_4 solution at room temperature in a potential region corresponding to hydrogen evolution reaction (HER). The start potential in CV was fixed at the open circuit potential (EOCP) after the electrode was immersed in the solution during 5 minutes. Prior to use, the solution was purged with argon for at least 30 minutes.

3. RESULTS AND DISCUSSION

3.1. Thermal effects on the crystalline phase of TiO_2

The XRD spectrum of the as-prepared sample (Fig. 1) shows an anatase phase with crystalline size about 5±2 nm, calculated by Scherrer´s equation. The anatase content and crystalline size for all samples investigated are shown in Table 1.

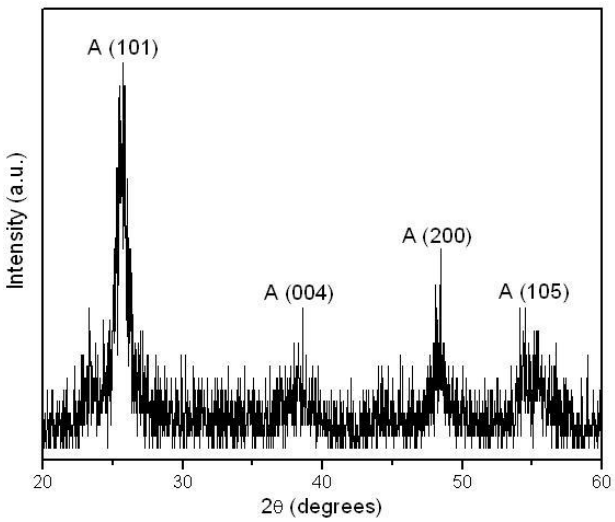

Figure 1. XRD spectrum of the as-prepared sample. All the peaks were indexed according to JCPDS 21-1272 for the structure of anatase.

From the analysis of the thermal effect, the XRD spectra (Fig. 2), shows that below to 550 ºC all peaks belong to the anatase phase and no other phase is detected within the X-ray detection limit. Our attention was focused on the inspection of the temperature interval from 550 to 750 ºC, where the

anatase was found to undergo a phase transition to the stable rutile form. The XRD spectrum of the sample heated at 550 ºC reveals the anatase (101) and emerging diffraction peak of rutile (110), indicating that the sample heated at 550 ºC is a mixture of anatase and rutile (91.75 and 8.25, respectively). Therefore, the phase transformation to the rutile structure takes place when the temperature is raised at least above 550 ºC. Between 800 and 900 ºC the main crystalline structure is rutile.

Table 1, indicates that onset of anatase-rutile phase transition initiate the anatase nanocrystals coarsen and their size reaches a critical particle size (~35 nm) and then transform to stable rutile phase. The experimental results suggested that the thermodynamic driven force for anatase-rutile transformation comes from the high surface energy and redistribution of energy in the system.

With the primary crystalline size of as-prepared sample the nucleation sites will increase due to large specific surface area and consequently the transformation rate will be increased as temperature was increased. Thus, one should consider two competitive processes in the nanocrystalline anatase powders thermally treated at a higher temperature: grain growth and phase transformation, which both occur more readily in smaller grain samples. Therefore, the coarsening mechanism can be analyzed as two kinetic domains, in the first domain anatase has two functions, (1) coarse and (2) transform to rutile, in the second domain rutile is identified and has the sole function of coarsening progressively.

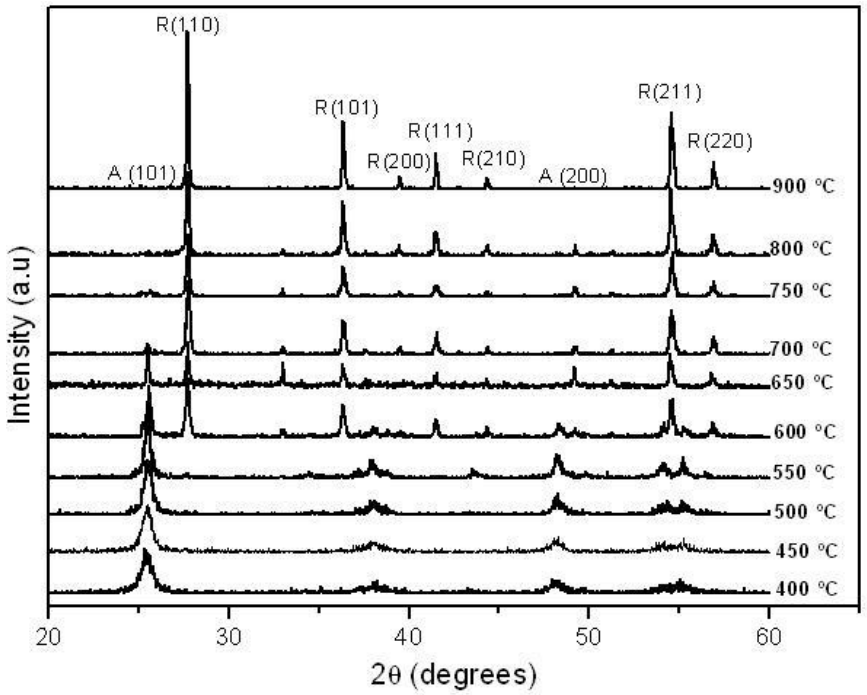

Figure 2. XRD spectra of the heat treated samples at different temperatures for 2 hours, *A* and *R* meaning anatase and rutile phase, respectively.

Analyzing Fig. 3, it can be observed that up to 500º C the main crystallite phase was anatase, whose diffraction peaks were sharpened with increasing heat-treating temperature. At 550º C, a trace of the (110) diffraction peak of rutile phase is observed, indicating that at this temperature the sample

has a mixture containing 91.75% of anatase and 8.25% of rutile with a crystallite size of about 35 ± 2 nm and 30.50 ± nm, respectively (see Table 1). After heating at 550º C, the rutile phase increases its percentage steeply up to 100% at 800º C, without any trace of anatase phase.

At temperatures between 550º C and 750º C, there are mixtures of anatase and rutile phases and the intensity of the rutile peak (110) increased significantly while that of anatase peak (101) decreased. After heating at 750º C, the anatase peak (101) disappears and a single rutile phase is observed. The rutile phase exhibits sharp XRD peaks without signs of broadening: this description is depicted clearly in Fig. 2.

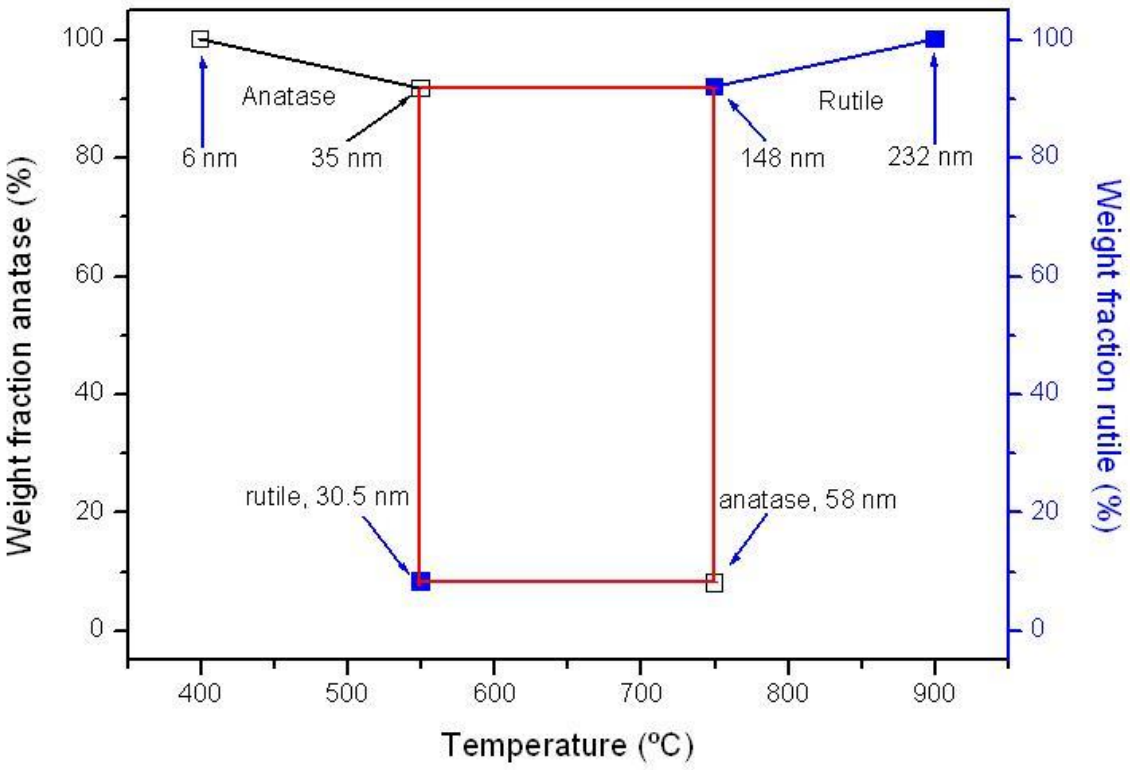

Figure 3. Dependence of crystallite size and weight fraction of anatase during the phase transformation as a function of the temperature.

Raman spectroscopy was used in addition to the XRD in order to find evidence of the structural phase and to gather information about Raman spectrum of the as-prepared sample, which is shown in Fig.4 (a). A well resolved Raman peak is seen at 143 cm^{-1} (E_g) and three broader peaks are found in the high frequency region located around 398 cm^{-1} (B_{1g}), 515 cm^{-1} (A_{1g}) and 637 cm^{-1} (E_g). These bands observed in the spectra are close to those in the bulk anatase phase [12]. Fig .4(a), evidenced that the spectrum of the as-prepared sample has the long-range order of the anatase phase, a fact which confirms the results obtained by XRD. Fig. 4(b) shows the bands broaden with respect to the full width at half-maximum (FWHM), which may be due to the scattering and size effects.

Furthermore, RS was introduced to investigate the anatase- to-rutile phase transformation in the samples heat-treated because this spectroscopy is much more sensitive detection of nanosized

crystallite domains as compared with XRD. When observing the RS as a function of heat treating temperature, it becomes evident that heat treating can stabilize the porous framework of the as-prepared sample, Fig. 4(b). The observed Raman bands were assigned to the anatase and rutile form of TiO_2 in accordance with the literature [13,14]. The Raman spectra at low frequencies assigned as E_g mode, for anatase phase become stronger at higher temperatures, indicating the enhancement of long-range order, which means that the number of atoms (Ti and O) forming molecules of anatase also increases. This indicated that anatase phase was still forming during heat treatment, which is consistent with a coalescence mechanism, rendering coarser grains and the reduction in specific surface area, as was already analyzed. Between 400 and 550 ^oC, only bands of the anatase phase were observed with higher intensity as the heat treatment temperature increased, indicating the enhancement of long-range order with increasing heat treatment temperature.

As the latter increases up to 600 ^oC, a peak at around 441 cm^{-1} and a shoulder at around 607 cm^{-1} appeared, these bands are the E_g mode and $A1_g$ mode of the rutile phase, respectively. Between 550 and 600 ^oC, the presence of rutile Raman modes indicate that rutile phase stars to form in this temperature range.

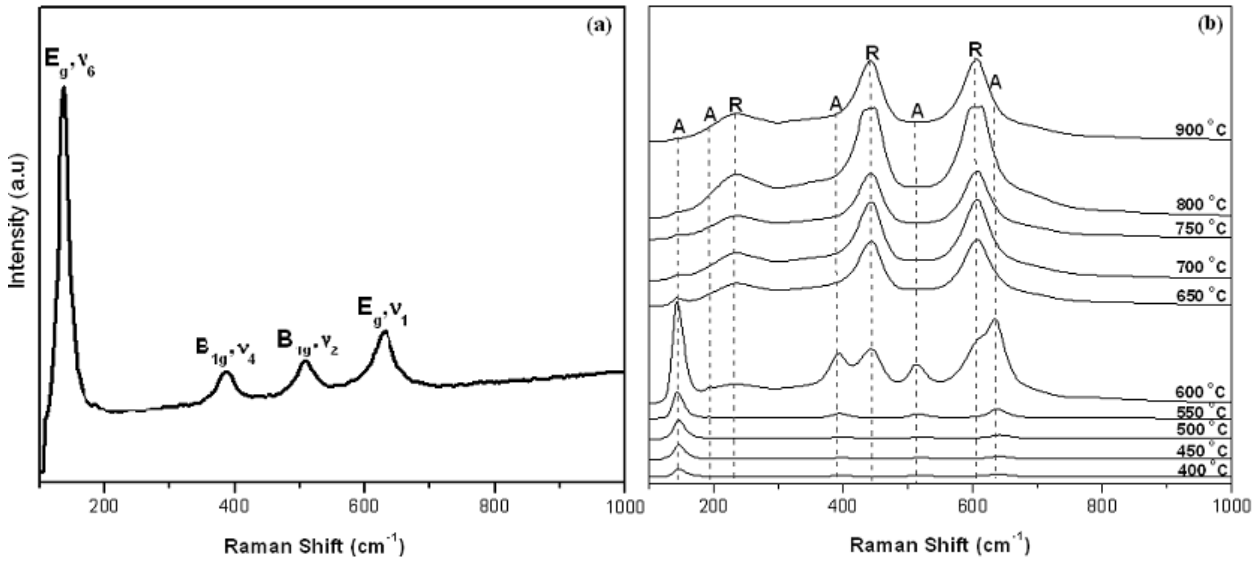

Figure 4. (a) Raman spectrum of the as-prepared sample, (b) Raman spectra of the heat treated TiO_2 samples showing the phase transformation anatase-to-rutile. The Raman features of anatase and rutile phases are denoted as A and R.

At 800 and 900 ^oC, the entire anatase features have been completely wiped out with only the presence of rutile features, indicating the completion of the anatase-rutile transition. Therefore, it is evident that anatase to rutile transformation can proceed with increasing heat treatment temperature. This fact suggests that the anatase-rutile transformation is directly associated with a diffusion mechanism.

In anatase single crystals, it was observed that the rutile phase nucleated at the surface and spread internally into the anatase phase during the phase transformation. This fact may indicate that

rutile has a lower surface energy compared to that of the anatase phase. In the nanophase, the surface region is formed by a high defect density where atoms relax from their normal lattice sites. It is more favorable for the rutile phase to nucleate at this imperfect surface so as to lower the total free energy of the system. The Figure 5 shows N_2 adsorption-desorption isotherm and corresponding pore-size distribution plot (inset) of the as-prepared sample. All isotherms (as-prepared and thermally treated, no showed herein) could be classified as type II category, indicating the presence of capillary condensation in the mesoporous structure. The subsequent rise of the thermal treatment temperature the mesoporous and the total BET surface area reduced drastically as result of heat treated and densification. The anatase-rutile transformation is associated with crystallization and leads to change of microstructure characteristics. The BET surface areas of the samples thermally treated determined from the nitrogen adsorption-desorption isotherm by the BET (Brunauer-Emmet-Teller) method are summarized in Table 1.

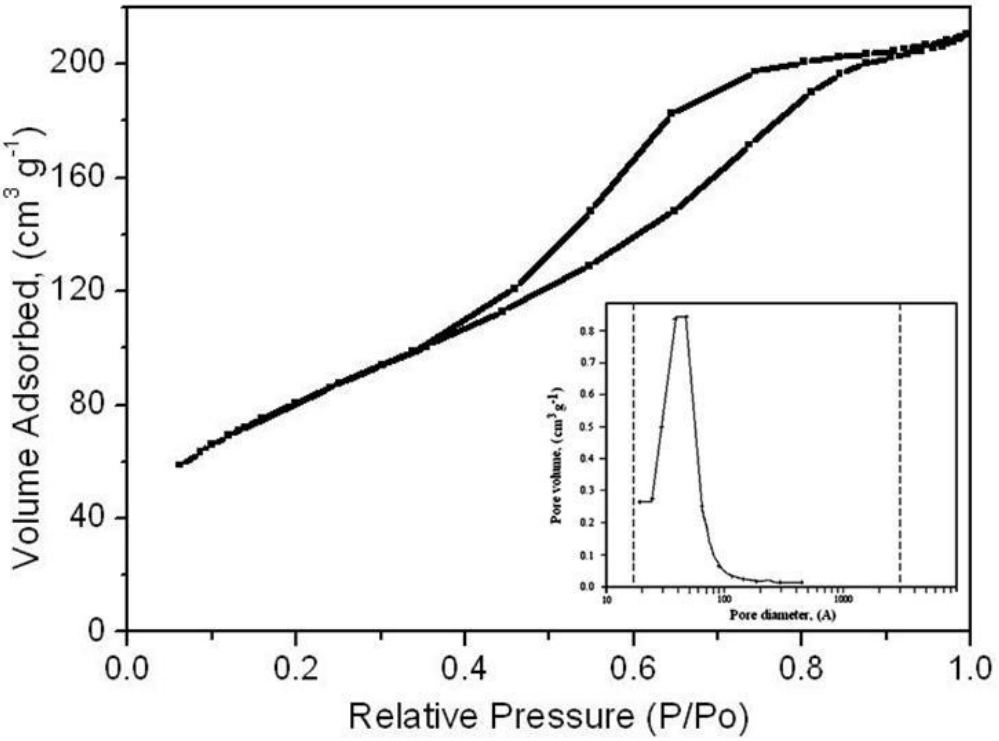

Figure 5. N_2 adsorption-desorption isotherm of as-prepared sample and corresponding pore-size distribution plot (inset).

The UV-vis absorption spectrum from the as-prepared sample is show in Fig. 6. The as-prepared sample exhibits a blue shift in the absorption edge ($\lambda_{as\text{-}prepared}$= 412 nm), due to the so-called quantum size effect, which can be observed as higher energy shift in the optical bandgap or exciton energy [15]. The samples thermally treated exhibit a systematic "red-shift" in the absorption edges with the increase of experimental temperature (no showed herein). The direct transition can be estimated from a plot of α^2 versus E_{phot} photon energy (hv) and $(\alpha hv)^2$ versus photon energy (hv), respectively.

In order to establish the type of band-gap transition in the as-prepared sample, the direct bandgap transition can be estimated from a plot of $(\alpha hv)^2$ versus photon energy (hv) as shown in Fig. 6 (inset). Figure 6 shows the $[F(R)hv]^2$ versus Photon Energy (eV) for an direct transition (inset). The interception of the tangent to $[F(R)hv]^2$ =0 the plot will give a good approximation of the band-gap energy at 3.31 eV for the as-prepared sample due the so-called quantum effect. The indirect transition plot, not showed herein, fit plot yield band gap value of 2.96 eV which does not seem reasonable according to quantum size effects which can be responsible for the larger band-gap of the as prepared sample. As can be seen from the band-gap value in Table 1, the band-gap shifts estimated for the as-prepared sample from the plot for indirect transition are lower than 3.2 eV in bulk TiO_2 samples and therefore it could be inferred that the direct transition is more appropriated to explain this behavior. The band-gap value for the as-prepared sample indicates that its electronic properties changed due to small crystals of TiO_2 (see Table 1). Table 1 shows the band-gap (direct and indirect transition) that is given by the intercept of the line with the photon energy axis. This Table indicates that the energy of the lowest excited state of as-prepared sample and heat-treated depend on their size: the smaller the size the higher energy. This effect is manifestation of the quantum size effect. Also, suggests that the direct, and not indirect band-gap, is more favorable in TiO_2 nanoparticles. The results, also, can be explained by the volume conservation law, which states that increase in the one lattice constants should be compensated by a decreased in the other one, and vice-versa, as it is the case in the low-energy regions.

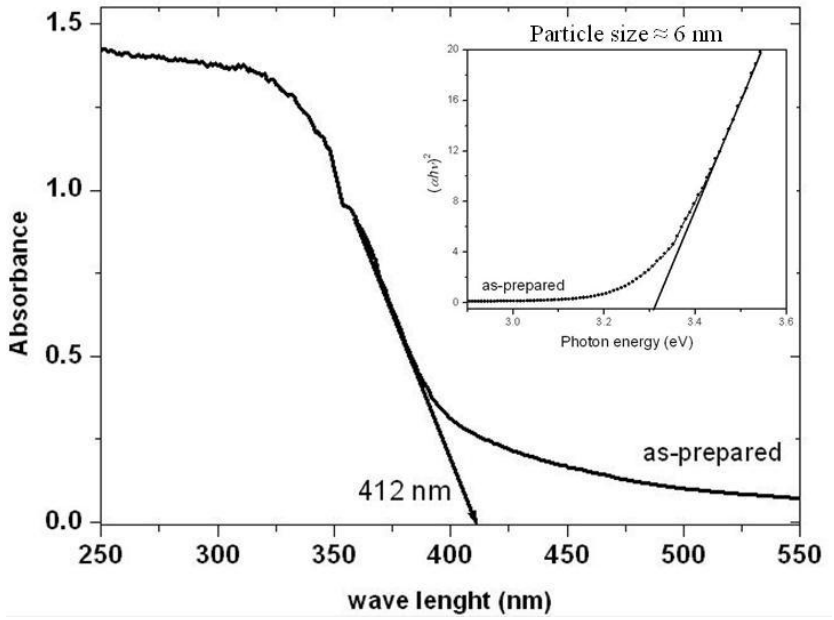

Figure 6. UV-vis diffuse reflectance spectra and plot $(\alpha hv)^2$ vs. photon energy (inset).

Therefore, the anatase as well rutile show an almost linear increase of the band-gap width when decreasing the volume or increasing lattice constant *a*. In fact, to achieve a smaller band-gap the lattice constant *c* has to be compressed and *a* has to be expanded [16]. Also, for direct band-gap in TiO_2,

electronic transition from the valence band to conduction band is electrical dipole allowed and the electronic absorption as well as emission is usually strong. For indirect band-gap in TiO_2, the valence band to the conduction band electronic transition is electrical dipole forbidden and the transition is phonon assisted, i.e. both energy and momentum of the electron-hole pair are changed in the transition. Both their absorption and emission are weaker compared to those of direct band-gap in TiO_2, since they involve a change in momentum.

In order to have evidence of the changes on the morphology, SEM analysis have been carried out on the sample heat treated at 400º C (Fig. 7), where it reveals the presence of spherical particles. Also, it shows that the nanostructured anatase phase started the coarsening process in which the anatase particles in contact with another form a neck and bond together, which minimizes the total surface energy by diffusional mass transport. According to the evidence showed in Fig. 7, one can establish that during the coarsening stage, the structure of anatase changed to fully satisfy requirements of equilibrium thermodynamics during the heat treatment temperature.

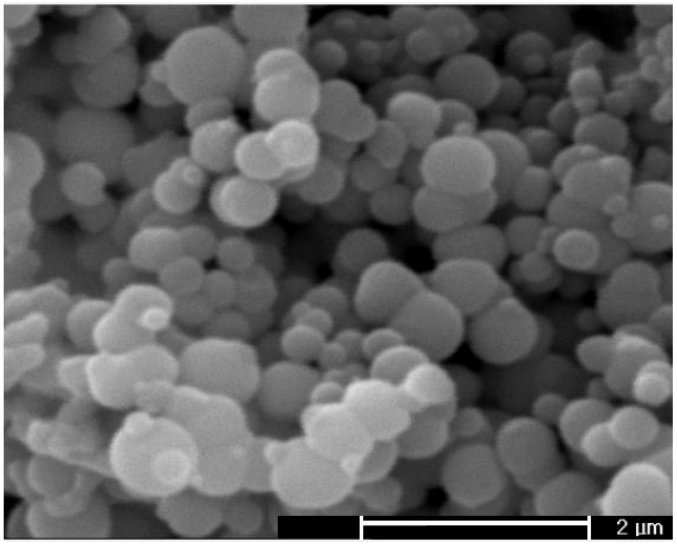

Figure 7. SEM image at 400º C of the as-prepared sample.

According, to the XRD, SR, S_{BET}, UV-vis diffuse reflectance spectra and SEM results it is possible to formulate a model of particle size evolution during the anatase-to-rutile phase transformation, which is presented in Fig. 8. The model proposed considers coarsening and growth of two particles of different sizes; this consideration is due to the collisions between the particles due to the shock waves via ultrasonic irradiation during sonochemical synthesis.

On the growth stage, particles of dissimilar size come into contact due to thermal diffusion, Fig. 8(a); as the starting particles are spherical in shape, long-range coarsening between different particles sizes is the primary mechanism for surface energy reduction due to thermal effects. Therefore, the short-range mass transport from the high-curvature region to the low-curvature region in the same particles is not significant. This changes the morphology of the anatase particle by dissolving small particles and transferring their mass to the larger particles, Fig. 8(b), As a result, the particle size

increases while the particle density decreases with heat treatment temperature. In Fig. 8(c), phases already coexist but they are separated by interfaces that grow at the expense of each other. In this stage an incipient rutile phase emerges in the parental material as a result of thermal fluctuations. Furthermore, Fig. 8(c) shows the coarsening process which is a slow mechanism of establishing global equilibrium with a complete anatase-to-rutile phase transformation. On the coarsening stage, the structure of the transformed phase changes to fully satisfy requirements of equilibrium thermodynamics. Therefore, all stages of the said phase transformation are subjected to thermal effects, which stem from the necessity to redistribute internal energy in the material undergoing the transformation.

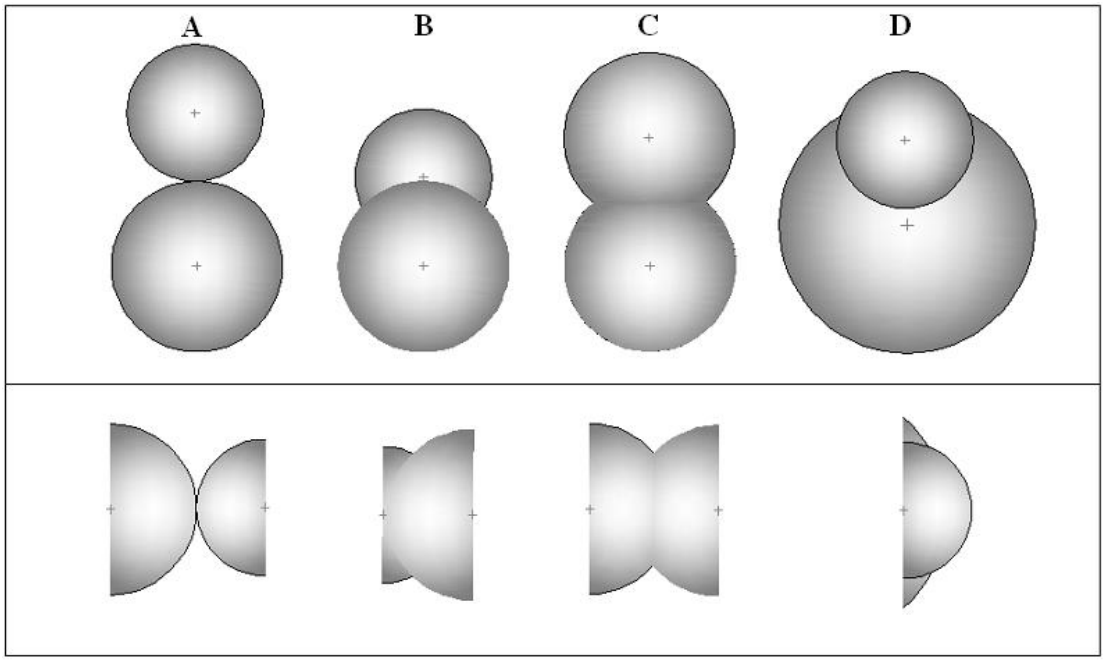

Figure 8. Schematic mechanics during the coarsening and grain growth due to thermal effect on TiO_2 nanoparticles of different sizes.

The average crystalline size of the as-prepared sample was confirmed by TEM micrographs and agrees with the XRD spectrum (Fig. 1). The select area electron diffraction pattern Electron diffraction pattern (SAEDP), (Fig. 9(b)), corresponds to the anatase phase. SAEDP confirms that the as-prepared is crystalline in nature such as can be confirmed observing, Fig. 9(a) and (c). The conventional dark field image shows brilliant nanoparticles which are oriented in the direction [101] related to anatase phase (Fig. 9(a)). Through HRTEM micrograph, Fig. 9(d) was determined the morphology of the as prepared sample and the nanoparticles lattice spacing is consistent with nanocrystalline anatase phase, JCPDS 21-1272. The average size of the crystallites was of the order of 5 nm. Fig. 9(e) shows a zoom of the Fig. 9(d), rectangle zone, showing that the as-prepared sample consist of nanocrystallites of anatase type structure and pores (arrow) at the junctions (circle) of crystallites. This observation is very important because crystal defects in semiconductors such as TiO_2 can influence the density of charge carriers and subsequently materials performance, for example in

photocatalysis. Therefore, is possible establish that no necessarily crystals with nanometric size and huge specific surface area are better for process such as photocatalysis, it means that a critical size with few crystal defects are necessary for increases the density of charge carriers. The Fast Fourier transforms (FFT) shows that the brightness and intensity of anatase crystals are well crystallized.

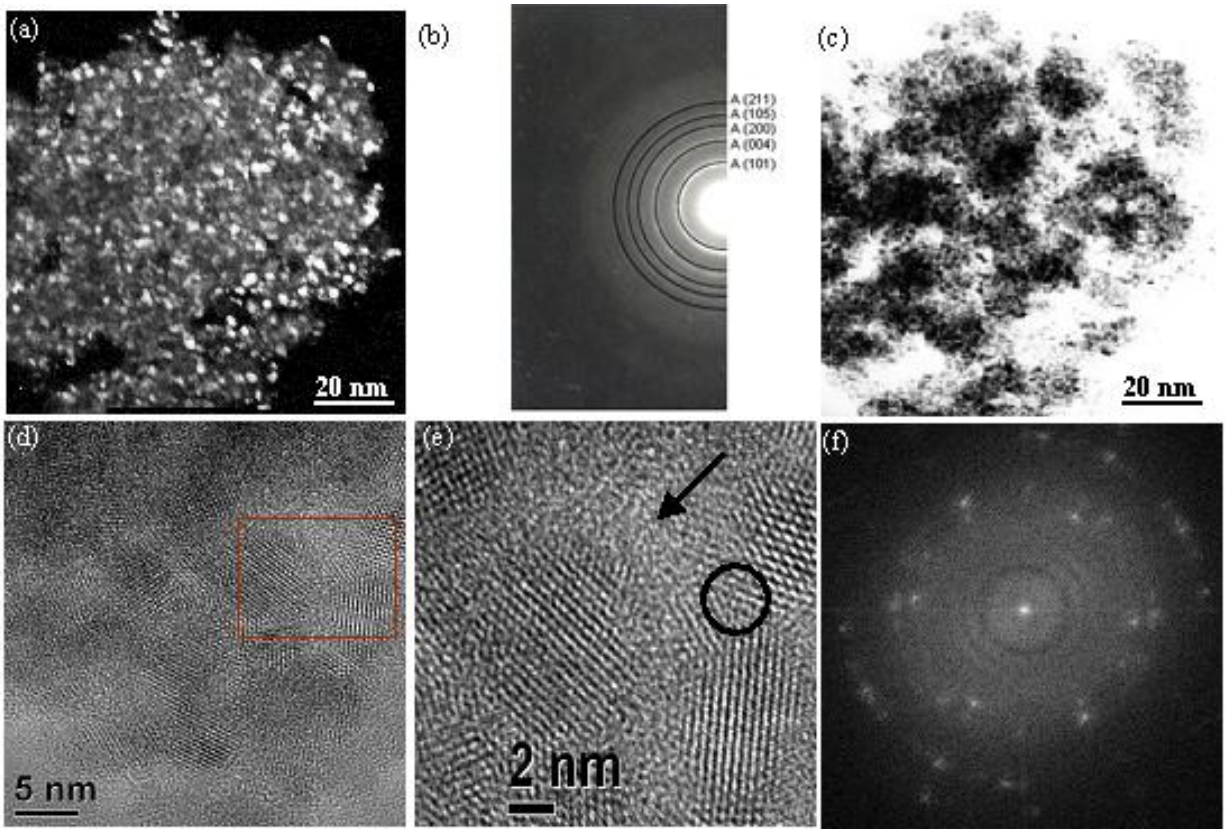

Figure 9. TEM-HRTEM micrographs of TiO_2-as-prepared. TEM Fig. 9(a), conventional dark field. Fig. (9b), electron diffraction pattern, and Fig. 9(c) bright field. HRTEM. 9(d) denoting the polycrystalline nature of anatase phase, select area of Fig. 9(e) emphasizing the crystalline structure and crystal size obtained by sonochemical, 9(f) the corresponding FFT.

The fig. 10 displays the current-charge evaluating of the as-prepared sample (100% anatase), 450 ^{o}C (100% anatase) and 900 ^{o}C (100% rutile) electrodes after the discharge and charge cycle. All the i-E characteristics were carried out in 0.5 M H_2SO_4 solution at room temperature. Excellent reversibility has been observed for all samples under investigation, corresponding to structural changes. This fact confirms that particle size lower than 20 nm, such as-prepared sample, has enough stability to allow the chemical reaction and shows reversibility. The CVs of anatase (as-prepared sample) and rutile (heat treated at 900 ºC) clearly indicates the differences in their HER voltametric response during the cathodic scan. In this region, a change on current densities for the as-prepared sample at 900 ºC (101.50 μA cm^{-2}) is observed. According to these characteristics, the rutile phase presents a slower HER kinetic compared to anatase phase. Therefore, micro-structural modifications during the phase transformation (anatase to rutile) are accompanied by changes in the electrochemical

behavior; indicating that a strong inhibition of the electron transfer process occurs, in agreement with the nature of TiO_2 [17].

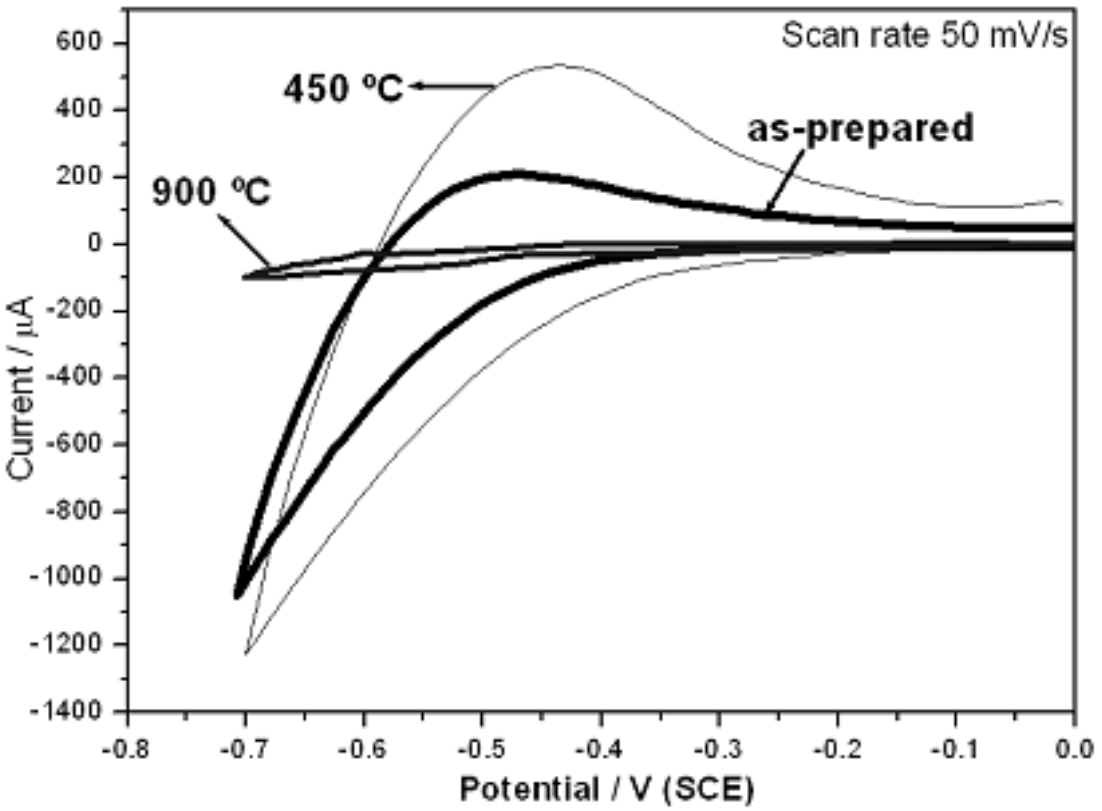

Figure 10. Cyclic voltammograms of original sample (anatase 100%), at 900 ºC (100% rutile) and 450 ºC.

The results discussed above are qualitatively consistent with the microstructural properties reported in the Table 1. The results suggest that the properties of nanosized semiconductor particles depend very sensitively on the particle size. For clusters in such a nano-metric size regime, a large percentage of atoms are on or near the surface and this fact is according to specific surface area for anatase obtained through sonochemical process (300.30 m^2g^{-1}) and compared to rutile phase obtained for heat treatment at 900 ºC (24.68 m^2g^{-1}). Under these conditions, the existence of vast interfaces between the cluster and the surrounding medium could produce a profound effect on the clusters properties and in consequence on the i-E characteristics.

In addition, Table 2, shows that the highest current-charge magnitude is presented in the sample with a heat treatment at 450 °C as mentioned. Hence, there is an optimal size (17nm), with particular structural and morphological properties, to improve electro-reduction processes such as water reduction [18]. The present study also clearly indicates that the micro structural changes directly influence the efficiency of the TiO_2 particles and the proton adsorption at the electrode interface.

Table 1. Anatase content, BET surface area, crystalline size and electrochemical characteristics as function of heat treatment temperature

Sample	Anatase content (wt%)	Cristalline size (± 2 nm)		BET surface area (m^2g^{-1})	Band-gap (Direct transition) (eV)	Band-gap (Indirect transition) (eV)	Current (μA)	Charge (μC)
		Anatase	Rutile					
As-prepared	100	6.4	—	300.30	3.31	2.96	1050	2759
400 ºC	100	11.80	—	240.30	3.24	3.03	1250	5037
450 ºC	100	17.30	—	198.32	3.22	3.04	1227	5884
500 ºC	100	21.90	—	157.48	3.20	3.04	666	2397
550 ºC	91.75	35	30.50	112.39	3.13	2.95	360	1483
600 ºC	42.51	43.30	59	75.69	3.02	2.90	102	278
650 ºC	36.70	56	94	60.09	3.00	2.89	109	390
700 ºC	8.56	89	121	40.15	3.00	2.89	47	173
750 ºC	8.05	58	148	32.31	2.99	2.89	176	522
800 ºC	0	—	194	30.41	2.99	2.89	228	802
900 ºC	0	—	232.20	24.68	2.98	2.90	101.50	325

Table 2. The result current-charge that when rutile phase has a difference in size higher than 30% respect to anatase phase, rutile has a superior electrical resistance, and such as result inhibit el current flux in the samples.

Cristalline size (± 2 nm)		Delta size* (nm)
Anatase	Rutile	
35	30.50	0.143
43.30	59	-0.372
56	94	-0.679
89	121	-0.360
58	148	-1.155

$\Delta r^* = (_{ranatase\text{-}rrutile)/ranatase}$

* The negative value meaning that rutile phase is greater than anatase phase

In particular, Table 2 highlights that when anatase and rutile are simultaneously present they show a decrease in conductivity. At certain values of particle size of rutile a decrease in conductivity is observed. Comparing particle size of anatase and rutile, we can observe that when this difference is about 35% of the current and has its minimum values, which indicate that the conduction and valence band could be farther away from the sample into two phases coexist when taking these sizes. The explication of these phenomena would be to see the interactions between the borders of particles that could be considered later.

This clear size-dependent evolution over electrochemical properties as function of phase transformation anatase-rutile was demonstrated. The rutile phase evolves lower induced charge density

inside the particle. The low current density of the as-prepared sample, could be limited by superficial defects being responsible of the complex network caused by a huge specific surface area (300.30 m^2g^{-1}), and could be included that TiO_2 belongs to the class of materials with very low drift mobility of electrons. This behavior lead to limited electron transport.

4. CONCLUSIONS

Nanostructured TiO_2 powders (5 ± 2 nm) were successfully prepared by a facile and environment-friendly sonochemical route. The critical nuclear-size value to start the phase transformation anatase-to-rutile phase was 35 ± 2 nm and 30.50 ± 2 nm for anatase and rutile phases, respectively.

An optical band gap of as-prepared sample increases to 3.31 eV respects to 3.20 eV and shows a direct transition. This expansion can be attributed to the quantum size effect which can be observed as a blue shift in the UV absorption spectrum. Also, in this case, the band gap increases due to the expansion of the lattice constant *c*. while the lattice constant *a* has the smaller value than the bulk and this can be explained by the volume conservation law. The apparent kinetic limitation of the hydrogen evolution reaction (HER) could be related to the size of each active site, porosity and lattice defects on the samples. These features directly influence the electrochemical properties of TiO_2. This fact is confirmed because the highest current-charge magnitude, in the cathodic region, is presented in the sample with a heat treatment of 450°C with crystalline size of 17 nm, specific surface area of 198.32 (m^2g^{-1}) and current density of 1250 μA cm^{-2} versus as-prepared sample (1050 μA cm^{-2}) with specific surface area of 300.30 m^2g^{-1}. The large specific surface area could be produced the presence of trapped electrons and holes that, in turn, modify the electrochemical properties. Also, there is an important influence on the structural and morphological evolution of the original sample produced by heat-treated temperature.

ACKNOWLEDGEMENTS

The authors gratefully acknowledge to CONACyT-SNI for the distinction of their membership and the stipend received. Héctor Herrera H. also would like to thanks INNOVA INVESTIGACION S.A. de C.V. for its materials support during the electrochemical experiments.

References

1. Ji-Guang Li, Hiroshi Kamiyama, Xiao-Hui Wang, Yusuke Moriyoshi, Takamasa Ishigaki, *J.Eur. Ceram. Soc.*, 26 (2006) 423.
2. D.F. Ollis, E. Pellizzete, N. Serpone, *Environ. Sci. Technol*., 25 (1991) 1522.
3. W. Li, C. Ni, H. Lin, C. P. Huang, S. Ismat Shat, *J. Appl. Phys*., 96 (2004) 6663.
4. Yin Li, Suo Hon Lim, Tim White, *International Journal of Nanoscience*., 3 (2004) 749.
5. Hamed Arami, Mahyar Mazloumi, Razieh Khalifehzadeh, S.K. Sadrnezhaad, *Mater. Lett*., 61 (2007) 4559.

6. Yang Liu, Yan Li, YuntaoWang, Lei Xie, Jie Zheng, Xingguo Li, *J. Hazard. Mater*., 150 (2008) 153.
7. Kenneth S. Suslick, Millan M. Mdleleni, Jeffrey T. Ries, *J. Am. Chem. Soc*., 119 (1997) 9303.
8. Neppiras, ,E. A. Noltingk, B.E, *Proc. Phys. Soc*., B64 (1951) 1032.
9. Kenneth S. Suslick, *Science*., 247 (1990) 1439.
10. Leonardo González-Reyes, I. Hernández-Pérez, Francisco C. Robles Hernández, Hector Dorantes Rosales, Elsa M. Arce-Estrada, *J.Eur. Ceram. Soc*., 28 (2008) 1585.
11. Spurr, R.A., Myers, H, *Anal. Chem. Res*., 29 (1957) 760.
12. Balachandran, U, Eror, N.G, *J. Sol. State Chem*., 42 (1982) 276.
13. Leonardo González-Reyes, Isaías Hernández-Pérez, F.C. Robles Hernández, *Chemical Engineering Science.*, 66 (2011) 721.
14. Toshiaki, O.Fujio I, Yoshinori F, *Raman Spectrosc*., 7 (1978) 321.
15. Y. Wang, N. Herron, *J. Phys. Chem*., 95 (1991) 525.
16. K. Madhusudan Reddy, Sunkara V. Manorama, A. Ramachandra Reddy, *Materials Chemistry and Physics.*, 78 (2002) 239.
17. Diebold, U., *Surf. Sci*., 48 (2003) 53.
18. W.J. Ren, Z.H. Ai, F.L. Jia, L.Z. Zhang, X.X. Fan, Z.G. Zou, *Appl. Catal*., B69 (2007) 138.